A laboratory system for single-point multidirectional loading and 3D motion reconstruction

A.R. Mehrabadi
University of Southampton, Southampton, United Kingdom, A.rashidimehrabadi@soton.ac.uk

Q. Li, J. Mendoza, B. Cerfontaine, D.J. White, S. Gourvenec
University of Southampton, Southampton, United Kingdom, j.mendoza-ulloa@soton.ac.uk, B.Cerfontaine@soton.ac.uk, david.white@soton.ac.uk, Susan.Gourvenec@southampton.ac.uk

ABSTRACT: This paper describes a specialised laboratory system that enables single-point multidirectional loading with real-time three-dimensional displacement monitoring. The rig combines a load cell, a low-friction 360° self-aligning swivel pulley, a rigid measurement platform, and three linear displacement transducers, and attaches to an XYZ rectilinear actuator. In operation, the XY axes are used to position the Z-axis in plan relative to the foundation, and a single loading line running from the Z-axis around the rotating swivel applies general cyclic loading, via feedback control, to the foundation. Three-dimensional anchor head displacements are reconstructed via spherical-intersection (trilateration) applied to the linear displacement transducer data. System verification activities are presented, including (i) micrometre-imposed steps with 20 μm graduations and (ii) replication of a prototype anchor head trajectory derived from finite-element analysis scaled to centrifuge conditions. In both cases, reconstructed motions closely match the reference values with sub-0.03 (mm) errors. The apparatus provides a compact, line-of-sight-independent solution for enclosed soil boxes and centrifuge testing, enabling reproducible multidirectional loading and accurate 3D motion reconstruction. This technology is relevant to shared anchor design in floating offshore wind and other geotechnical challenges involving multidirectional cyclic loading.

1 BACKGROUND

Shared or multi-line anchors for floating offshore wind introduce multidirectional loading to the anchor arising from changing wind-wave and current conditions and load redistribution across mooring lines (Fontana et al. 2016, Rose 2023, Coughlan et al. 2025, Lovera et al. 2025).

To characterise the change of direction, the resultant load acting on the anchor head is defined by the in-plane direction as α, and vertical load inclination as β (Figure 1).

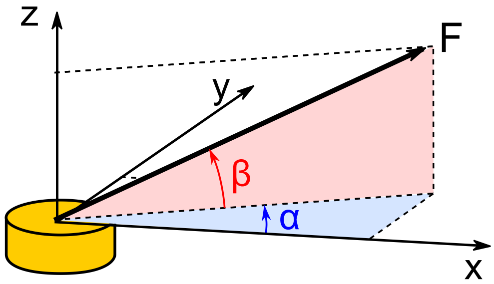

Figure 1. Definition of resultant load components in a spherical coordinate system; resultant load magnitude (F), in-plane direction of resultant load (α), vertical inclination of resultant load (β) (White et al. 2026).

In this study, multidirectional cyclic loading means cyclic histories in which both $\alpha(t)$ and $\beta(t)$ vary in response to co-linear or non co-linear wind, wave and current forces acting on floating wind turbines. Integrated aero-dynamic simulations by several authors demonstrate the resulting load variations. Typically, the magnitude of steady load is in the range $30-40\%\ U_{ult}$ where U_{ult} is the monotonic load at which the anchor's displacement reaches 10% of its diameter range. The in-plane angle, α, varies largely within $\pm 20°$ of the prevailing winds, waves and current directions. The vertical inclination of the resultant load, β can range between $10-60°$ depending on the mooring configuration and varies with standard deviation of $1-10°$ during operational or severe sea states (Pillai et al. 2022, Rose 2023, Coughlan et al. 2025, Lovera et al. 2025).

These ranges inform the design of loading paths in laboratory and finite element simulations. Geotechnical studies indicate that cyclic and multidirectional cyclic loading can alter the anchor stiffness, failure mechanisms and ultimate capacity (Herduin et al. 2016, Rashidi Mehrabadi et al. 2025). This challenge motivates the development of laboratory testing equipment that can impose controlled multidirectional load paths and measure anchor head motion in three dimensions with high fidelity.

Most existing laboratory implementations of multidirectional anchor loading use three mooring lines arranged around the anchor head and achieve multidirectionality by simultaneously controlling the three line forces and displacements to produce a resultant of prescribed magnitude and direction (Herduin 2019, Soriano-Camelo et al. 2024, Chalhoub et al. 2025). While effective, this approach typically requires reconfiguring the actuator layout for different loading directions. Also, this presents a real-time control challenge for maintaining both load magnitude and direction, because multiple actuators control the resultant load. These systems can be cumbersome and sensitive to rig compliance and backlash.

Accurate, continuous 3D tracking of the head of the anchor is essential for interpreting multidirectional responses. Recent solutions include (i) inferring motion from actuator encoders (e.g. Herduin (2019); Soriano-Camelo et al. (2024), (ii) orthogonal laser beams with reflectors (Soriano-Camelo et al. 2024, Chalhoub et al. 2025, Zabatta et al. 2025), and (iii) 6 DOF image tracking (Mohr et al. 2022). Each approach has advantages and limitations.

To select a displacement tracking approach suitable for tight spaces and long-duration cyclic programmes, we compared existing options against test-critical criteria (Table 1), which include:

- 2D/3D displacement reconstruction: Method can recover full 3D position (rather than only in-plane motion reconstruction).
- Line of sight: Requires an unobstructed optical path between sensor and target.
- Measurement correction: Raw readings require correction for line and rig compliance.
- Sensor follows the foundations: The sensing point is to be mechanically attached to and moves with the anchor head to reconstruct 3D head movements.
- Cost: Indicative hardware cost band for a lab setup (low $\lesssim £100\sim200$, medium $\approx £200-1000$, high $\gtrsim £1000$).

Table 1. Comparison of anchor head tracking options for multidirectional cyclic loading tests.

Method	2D/3D reconstruction	Line of sight	Measurements correction	Sensor follows the foundation	Cost
Lasers	2D/3D	Required	No	No	Medium
LVDTs	2D/3D	No	No	No	Low
String pot	2D/3D	No	No	Yes	Low
Encoder	2D	No	Yes	Yes	Low
6D tracker	3D	Required	No	Yes	High

The approach adopted in this study is the use of an array of three string potentiometers connected to the anchor head. This enables 3D reconstruction of displacement, within a tight testing space, and does not require corrections of measurement due to mooring line and loading rig compliance.

The system follows the anchor head under large deformations providing the opportunity to perform high number of cycles, and with a minimal cost of purchase and operation. In addition, the system does not obstruct the mooring line when transitioning through a wide range of direction and inclinations above the anchor.

This paper describes the development and validation of this integrated system to measure 3D anchor-head displacement under multidirectional loading. The paper (i) describes how multidirectional load is applied using a single mooring line and three actuator arrangement, (ii) presents how displacement is measured with a three-sensor tracking method and its calibration approach, and (iii) verifies the system accuracy through independent tests, demonstrating suitability for extended-duration multidirectional loading campaigns.

2 EXPERIMENTAL SETUP OVERVIEW

2.1 Mooring line orientation and loading

Figure 2 shows the rig used to apply multidirectional loading to the anchor and to track its three-dimensional response. The strongbox carries an XYZ actuator (three orthogonal actuators). The X and Y axes steer the loading origin in plan by controlling the position of the Z-axis, while the vertical movement of the Z-axis controls the applied load through an in-line load cell attached to the mooring cable. A low-friction, self-aligning 360° swivel pulley is mounted beneath the loading frame, taking the loading line through an angle from the vertical of the Z-axis to the direction of the anchor.

The pulley is fixed to a height-adjustable sliding rail so that the vertical inclination of the resultant force can be modified and set prior to testing within the range of $0° < \beta < 90°$. This value can also be adjusted during testing, via movement of the loading point along the Y axis.

The in-plane directionality can also be varied during the testing. Varying only the X axis allows a range of typically $-40° < \alpha < +40°$ from the initial direction of loading (depending on the value of β). If both traverse actuators are utilised (i.e. XY movement), a full sweep of in-plane directionality $\Delta\alpha = 360°$ is achievable, as well as variations from $0° < \beta < 90°$. The range is designed to represent the full potential range of vertical and in-plane angles reported in the literature for the resultant load of catenary or taut mooring conditions.

The mooring line runs from the load cell, around the pulley, and down to the anchor head where it is connected via a compact ball-top linkage. This linkage minimises secondary moments from the pad-eye connection and keeps the line colinear with the load reference point. Compared with multi-line actuation in prior work, which requires simultaneous closed-loop control of three lines and bespoke laboratory reconfiguration, this single-line architecture minimises rig changes and simplifies control. The trade-off is that this system requires larger actuator movements to create large changes in the resultant loading angle.

2.2 Measurement of anchor displacements

To measure the anchor head displacements, the self-calibrated string-potentiometer system offers a low-cost, line-of-sight-independent alternative that is well suited to enclosed boxes and extended testing.

A trilateration approach is adopted to interpret the three miniature string potentiometers arranged at 120° intervals around the anchor. At each instance, the position of the anchor head is reconstructed from the measured distance to three fixed points located around the box. When those three points are known and their distance to the anchor head is tracked continuously, the 3D position is determined reliably.

Since all three wires always follow the position of the anchor head, large displacements can be measured without the sensor falling out of range due to lateral movement (a problem commonly faced using fixed position laser or LVDT sensors). A schematic of the sensors is shown in Figure 3.

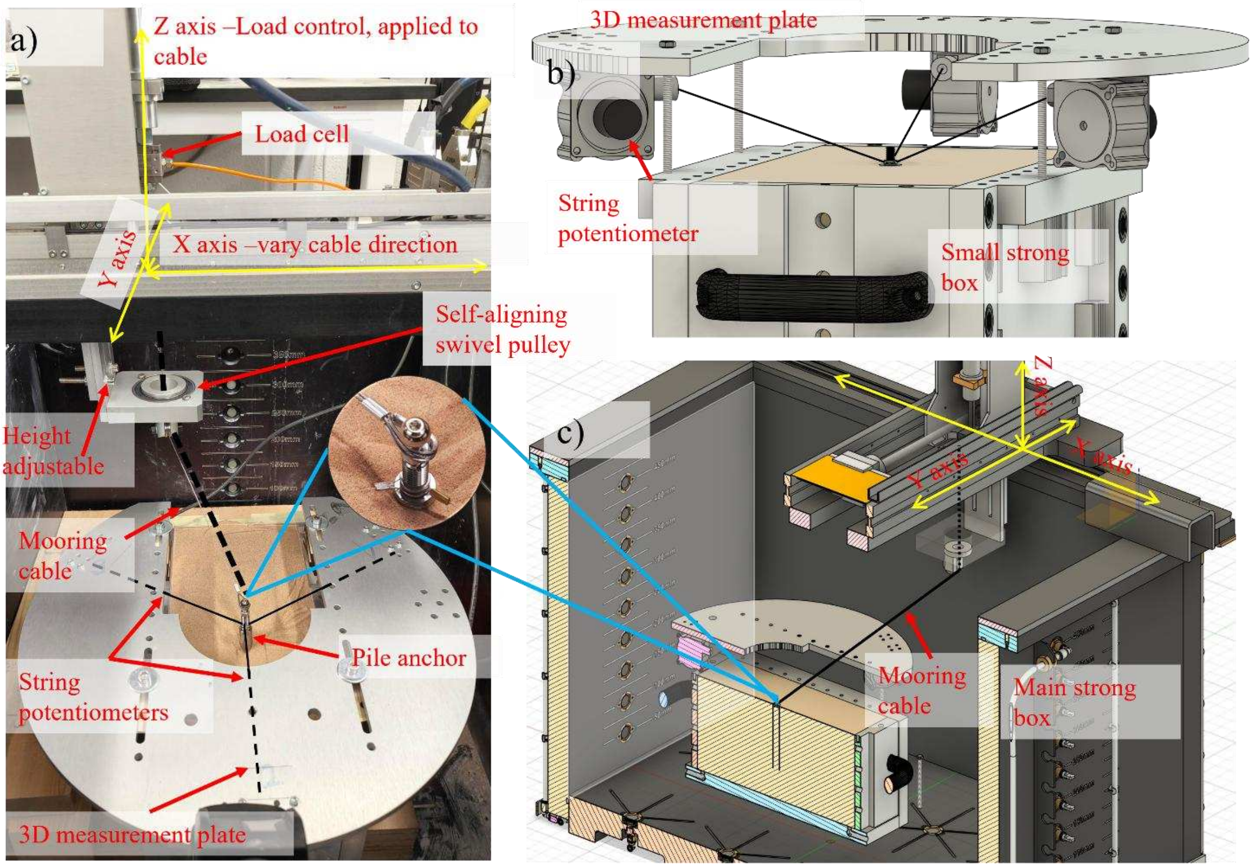

Figure 2. System overview: a) orthogonal X-Y actuators steer direction; Z actuator applied load; height-adjustable self-aligning swivel pulley sets vertical inclination; single mooring line connects to the anchor head through a ball-top screw linkage; b) three string potentiometers arranged around the anchor head underneath the 3D displacement tracking plate. c) Perspective view of the setup.

The sensors are mounted beneath a stiff, flat plate (referred to as the 3D measurement plate in Figure 2). The plate allows adjustment of the vertical inclination of the potentiometer wires (illustration Figure 2.c) by lifting or lowering the elevation of the plate prior to the test. Trials in the centrifuge show that the self-weight of the string does not lead to sag-induced error, but the spring return mechanism can be impaired at high g.

By increasing the wire vertical inclination (see Figure 2b), accuracy of the detection of vertical motion is improved and poor conditioning in the vertical direction is reduced. The plate is installed on the box after sand pluviation and before anchor installation to act both as a sensor support and as an installation template. The three strings converge to a common ring resting on the anchor head; the ring makes the wires move exactly with the anchor head, with no slip between the ring and the anchor head.

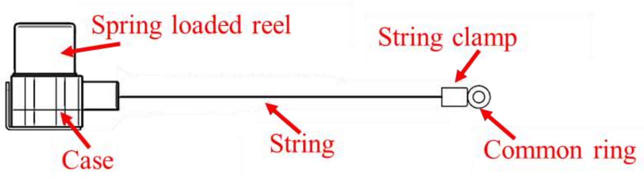

Figure 3. String potentiometer and anchor attachment ring

3 3D DISPLACEMENT TRACKING

3.1 Notation and geometry

Figure 4 defines the geometry and notation in plan (top) and elevation (bottom). The anchor-head position in the actuator frame is $P(t) = (x(t), y(t), z(t))$. The displacement origin is taken at the initial position of the anchor head, $P_0 = (x_0, y_0, z_0)$ with the assumed location of (0,0,0). The orientation of the cartesian axes aligns with the direction of the two orthogonal transverse actuators (x, y) as shown in Figure 4a The fixed (but initially unknown, within the tolerances of the assembly) base position of string potentiometer i is $C_i = (X_{R_i}, Y_{R_i}, Z_{R_i})$ for $i = 1,2,3$.

As noted before, the string potentiometers are arranged around the anchor head at 120° intervals. Also, due to the higher placement of string potentiometers relative to the anchor head, a vertical inclination angle, β, is formed between the wire and the horizontal plane. The in-plane direction of each string potentiometer taken from the origin is denoted α, and the vertical inclination of the wire to the horizontal direction is denoted β in Figure 4a and 4b. These angles are informative only and are not implemented in the equations of the displacement tracking system. The symbols are given in Table 2.

3.2 Geometry to solve anchor head position

The straight-line between the string potentiometer i and the current position of anchor-head is the length of wire i calculated by taking the norm of string-pot position C_i and anchor head $P(t)$:

$$L_i(t) = \|C_i - P(t)\| = \sqrt{(x - X_{Ri})^2 + (y - Y_{Ri})^2 + (z - Z_{Ri})^2} \quad (1)$$

The measurement from the potentiometer is $L_{i_{log}}(t)$, which differs from $L_i(t)$ by a constant offset o_i due to the clamped end length of the string which is not measured by the sensor (shown in Figure 2 and Figure 4c). This is constant for the string potentiometer used in this research at 14.2 (mm).

$$L_i(t) = L_{i_{log}}(t) + o_i \quad (2)$$

Repeating equation 1 for the three string-potentiometers gives three equations but twelve unknowns: three components of anchor head position, $P(t)$, and nine components of string-potentiometer base positions, $\{C_i\}^3 for\ i = 1,2,3$. Thus, to reconstruct $P(t)$ we must first establish the sensor bases C_i. Since the string-potentiometers are mounted on several manufactured brackets within a tolerance to the CAD drawing, direct measurement of C_i is limited by tolerances in manufacture. Also, dismantling and reassembly of the string potentiometers between tests changes their position. As a result, manual measurement of string potentiometer positions does not provide sufficient accuracy to reconstruct 3D anchor head displacement with high fidelity.

This problem is addressed by introducing a self-calibration procedure that uses the least-squares method on a predefined movement path to find the position of each string potentiometer in the coordinate system formed by three rectilinear actuators. By moving the actuators through a set of known displacements while the common ring is rigidly connected to the actuator (Figure 5) a path is recorded. Following the figure, the ring has moved from the starting point P_0, through the path and reached to the point P_k (Figure 4c). Then, using absolute-length differences:

$$\Delta L_i(k) = \|C_i - P_k\| - \|C_i - P_0\| = \|C_i - \Delta P_k\| - \|C_i\| \quad (3)$$

Since the data acquisition system is constantly collecting points on the path, N length difference equations (Equation 3) can be formed between the starting and any points on the path $\{\Delta P_k\}_{k=1}^{N}$. Stacking all the logged data points from the three sting potentiometers, we obtain $3N$ equations in the nine unknowns contained in $\{C_i\}$. We estimate the unknowns by minimizing a simple least-squares fit.

$$\min_{\{C_i\}} \sum_{i=1}^{3} \sum_{k=1}^{N} \left[\Delta L_{i,log}(k) - \Delta L_i(k)\right]^2 \quad (4)$$

Once C_i are known, the displacement data at each new time sample is reconstructed by solving the following equation using the least-squares method.

$$\min_{P(t)} \sum_{i=1}^{3} \left[L_{i,log}(t) - o_i - \|C_i - P(t)\|\right]^2 \quad (5)$$

Table 2. List of notations.

Symbol	Definition
$\boldsymbol{P(t) = (x, y, z)}$	Anchor-head position in the rectilinear actuators coordinate system at each time (t)
$\boldsymbol{C_i = (X_{R_i}, Y_{R_i}, Z_{R_i})}$	Base position of string-potentiometer in the rectilinear actuators coordinate system
$\boldsymbol{L_i(t)}$	True geometric distance from anchor head to string-potentiometer
$\boldsymbol{L_{i_{log}}(t)}$	Logged length of string-potentiometer
$\boldsymbol{o_i}$	Constant offset length due to clamped end

By executing known actuator movements and working with length differences (ΔL), the base-position identification step is turned into a simple least-squares fit in the actuator coordinates system. This ΔL method reliably finds the base points $\{C_i\}$, is offset-immune (the unmeasured length of strings (o_i) cancel in differences) and perfectly aligns the recovered string-pot geometry to the rectilinear actuator coordinate system. No manual ruler measurements or coordinate transforms are required, and it can be run quickly before each centrifuge test is assembled, providing a repeatable, pre-test self-check of the sensor geometry. This means that the assembled geometry of the system can be varied, which enables the use of sliding connection plates and spacer plates to adjust the absolute position and arrangement of the potentiometers, without needing to accurately measure the resulting coordinates.

The accuracy of the recovered string potentiometer base positions depends on how the predefined path excites the geometry.

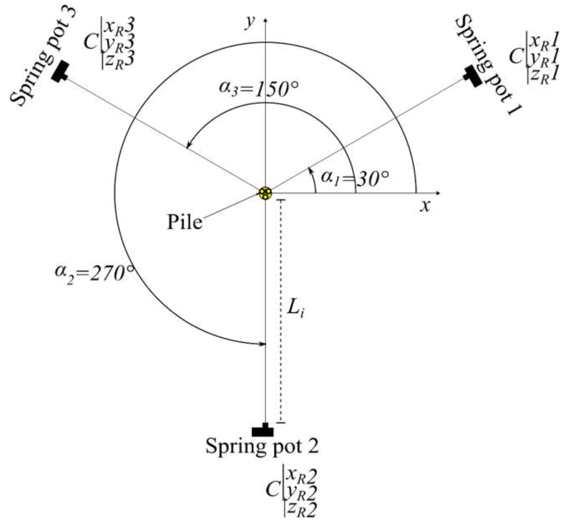

a) Plan view: three sensors arranged nominally 120° around the anchor head; unknown base positions Ci; instantaneous P(t); angle of each string-potentiometer measured from the x-axis origin α.

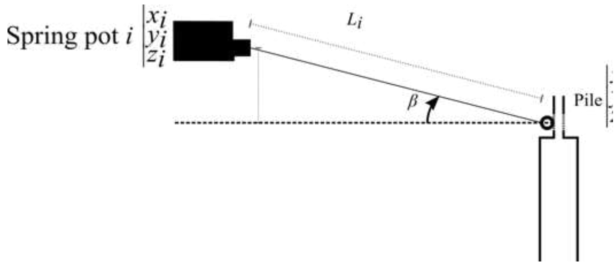

b) Side view: elevation of the sensor plate relative to the anchor head; angle of the potentiometer from the horizontal line (β) wire to increase measurement of vertical displacement accuracy.

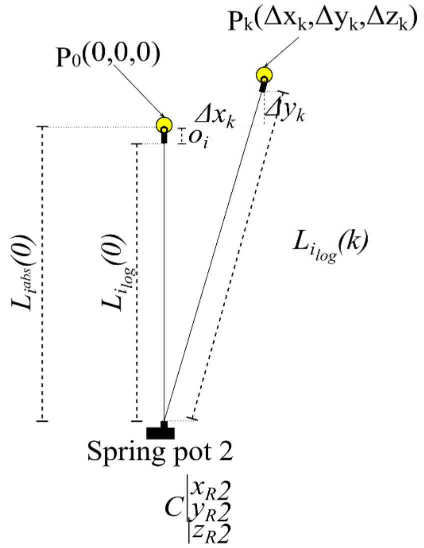

c) Plan view: displacement from the initial point P_0 to position P_k; actual length of wire (L_i); logged length of wire ($L_{i_{log}}$).

Figure 4. Geometry and notation used in the 3D displacement tracker formulation.

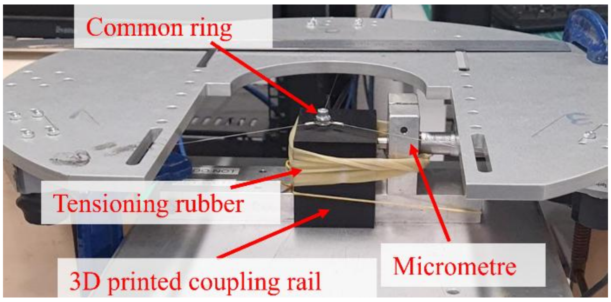

Figure 5. Setup for micrometre-imposed displacements. The common ring is coupled to a fixed micrometre via a rigid slider. The three string-potentiometer sensors are beneath the plate. The micrometre axis is aligned with the system x and y directions.

If motion is only along one axis (e.g., x only), the associated equations become nearly rank-deficient and only one component of the bases is well identified. Planar motion $(x + y)$ improves identifiability, and full 3D motion $(x + y + z)$ yields a well-conditioned system in which all components of C_i are recoverable with small variance. The calibration sequence therefore mixes steps in the x, y and z directions with small diagonals to avoid near-collinearity.

3.3 Verification by known 1D trajectories

To further quantify the accuracy and repeatability of the calibrated 3D tracking system, we imposed small, precisely known 1D displacements using a laboratory micrometre (10 µm graduations). The verification rig (Figure 5) comprises the sensor plate with the three string potentiometers mounted beneath, a fixed micrometre, and a 3D-printed sliding coupler that rigidly links the micrometre spindle to the common ring. A light tensioning rubber prevents separation, so the motion is transmitted without backlash. All data is reported in actual (model) scale units.

The micrometre axis was aligned first with the system x-axis and then with the y-axis using a laser for line-of-sight alignment. For each axis, a displacement sequence of 0 to 0.5 mm was applied in 20 µm increments. After reaching the maximum stroke, the motion was reversed back to the origin in the same step size. At every increment the three cable lengths were recorded by the data acquisition system. Using the calibrated base-point geometry, the anchor head proxy (common ring) position was reconstructed from the three lengths by a standard least-squares solution of the forward model.

Figure 6 a-b compare the induced micrometre displacement with the reconstructed displacement for the x and y-aligned tests, respectively. Both tests follow the 1:1 line closely across the full 0.5 (mm) range, with small, approximately zero-mean scatter.

The standard deviation of the reconstruction error is $\sigma_x = 0.0159$ mm for the x-axis and $\sigma_y = 0.0261$ mm for the y-axis. These error levels are well within the resolution required to resolve per-cycle ratcheting and other effects expected during multidirectional cyclic loading of anchor piles, as will be demonstrated in the next section.

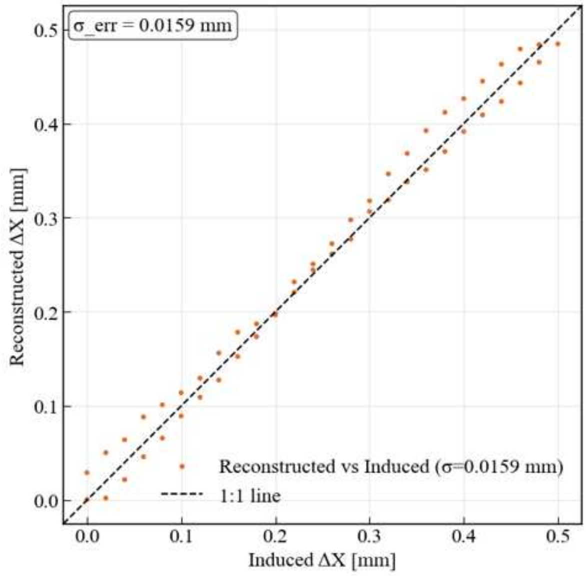

a) *x-axis alignment: standard deviation of reconstruction error $\sigma_x = 0.0159$ mm.*

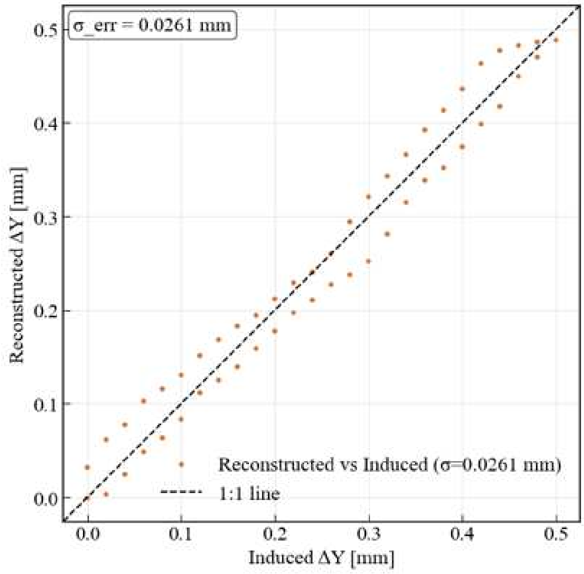

b) *y-axis alignment: standard deviation of reconstruction error $\sigma_y = 0.0261$ mm.*

Figure 6. Induced-reconstructed comparisons under micrometre steps of 20 µm up to 0.5 (mm) (forward and return sweeps). Reconstructed displacements (presented in model scale) closely follow the 1:1 line, with small, near-zero-mean scatter.

3.4 Verification with anchor trajectory

To evaluate the full measurement system analysis under a realistic, time-varying path, we imposed on the system a replay of an anchor head trajectory derived from an independent finite-element study of a 2.3 m prototype anchor pile subjected to multi-storm cyclic loading (Rashidi Mehrabadi et al. 2025).

The numerical displacement history was first scaled to centrifuge conditions assuming g=100 and then converted into an actuator motion time series. Because the simulated loading was planar, the replay used the vertical (Z) actuator and one horizontal (X) actuator. The common ring of the 3D tracking system was rigidly coupled to the actuators, and synchronous data were recorded from the two actuators and the three string potentiometer sensors.

Anchor head motion was reconstructed from the string potentiometer lengths using a standard least-squares trilateration at each time step. Figure 7 overlays the reconstructed trajectory and the actuator reference in $\Delta X\_\Delta Z$ space. The two curves coincide closely throughout the complex path.

Figure 7b reports axis-wise accuracy in two formats: (a) reconstructed vs actuator ΔX with a one-to-one line, and (b) reconstructed vs actuator ΔZ. The error standard deviation is $\sigma_x = 0.003\ mm$ and $\sigma_z = 0.013\ mm$. The larger error in Z arises from geometry.

During these tests the three string potentiometer bases were only ~30 (mm) above the anchor head, which weakens the vertical sensitivity and makes the estimation problem ill-conditioned in directions out of the horizontal plane that the potentiometer wires are closely aligned with. Raising the sensor plate (or adding a fourth oblique sensor) improves Z observability, but at the expense of working space around the anchor for multidirectional loading.

Overall, the replay confirms that the calibrated system tracks realistic prototype-inspired trajectories with sub-0.02 (mm) errors, adequate to resolve ratcheting and other small incremental effects in multidirectional cyclic campaigns.

4 CONCLUSIONS

This paper demonstrates a new integrated apparatus and methodology for laboratory simulation of multidirectional loading on anchors, combining a single-line, three-actuator drive with a self-aligning 360° swivel pulley and a self-calibrated, three string potentiometer displacement tracker.

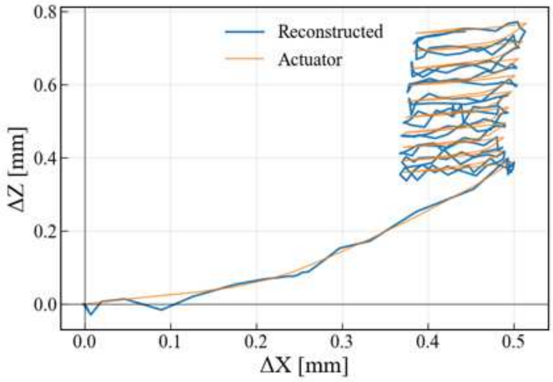

a) $\Delta X_\Delta Z$path: reconstructed vs actuator reference, showing close overlap along the full trajectory.

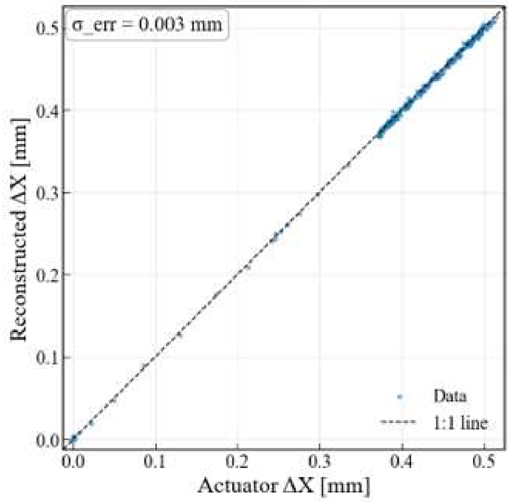

b) Axis-wise accuracy in X: reconstructed vs actuator ΔX with 1:1 line; $\sigma_x = 0.003\ mm$

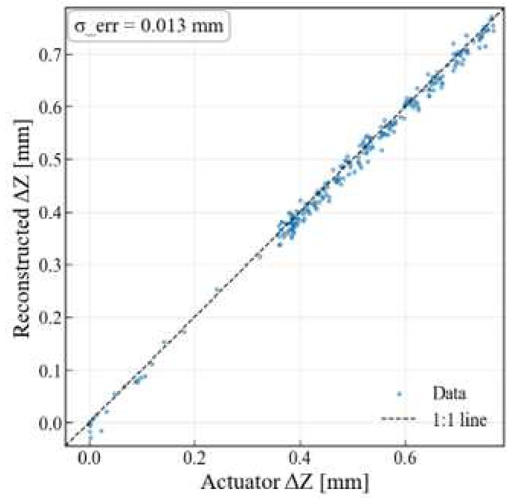

c) Axis-wise accuracy in Z: reconstructed vs actuator ΔZ with 1:1 line; $\sigma_z = 0.013\ mm$

Figure 7. Prototype-trajectory replay for system-level verification. Actuator time series derived from a scaled FEA trajectory (scaled down to model) of a 2.3 m anchor pile (g=100) were applied using the X–Z actuators; the anchor head motion was reconstructed from three string-potentiometer sensors.

The loading concept exploits an existing set of rectilinear XYZ actuators on a strong box without re-arrangement. Direction control reduces to prescribing the actuator trajectory, with the resultant force being co-linear with the loading line thanks to a swivelling pulley arrangement. For motion measurement, an offset-immune self-calibration step identifies the unknown sensor base positions directly in the actuator frame from prescribed moves, eliminating manual surveying and ensuring perfect frame alignment for subsequent tests.

Verification results demonstrate that the approach attains sub-0.03 (mm) accuracy under micrometre-imposed steps ($\sigma_x = 0.016\,mm$, $\sigma_y = 0.026\,mm$) and closely tracks a prototype trajectory replay derived from finite-element simulations ($\sigma_x = 0.003\,mm$, $\sigma_z = 0.016\,mm$).

This performance is sufficient to resolve per-cycle ratcheting and path-dependent behaviour during long, multidirectional cyclic campaigns. The system is low-cost, line-of-sight independent, and quick to re-calibrate, practical advantages for enclosed soil boxes and centrifuge operations.

5 ACKNOWLEDGEMENTS

This research forms part of TAILWIND, an EU Horizon Europe project with financial support provided by the European Commission (Grant Agreement 101136195) and by UK Research and Innovation (Project Reference 10108324).

Susan Gourvenec is supported by the Royal Academy of Engineering under the Chairs in Emerging Technologies scheme. David White is supported by the EPSRC Supergen Offshore Renewable Energy hub under grant EP/Y016297/1.

6 REFERENCES

Chalhoub, R., Jenck, O., Kochnev, A., Liaudat, J., Dano, C., Abadie, C., Szymkiewicz, F., Al Katabi, M. and Zachert, H. (2025). Floating wind turbine anchor piles under lateral multidirectional cyclic loading: experimental investigation. Proc. 5th Int. Symp. on Frontiers in Offshore Geotechnics (ISFOG 2025), pp. 2419–2425. http://doi.org/10.53243/ISFOG2025-209

Coughlan, K., Davis, M., Westgate, Z., Lee, J., Arwade, S.R., Martin, B. and DeGroot, D.J. (2025). Design and analysis of shared anchor layouts for floating wind farms in deep waters. Ocean Eng., 320: 120208. http://doi.org/10.1016/j.oceaneng.2024.120208

Fontana, C.M., Arwade, S.R., DeGroot, D.J., Myers, A.T., Landon, M.E. and Aubeny, C.P. (2016). Efficient multiline anchor systems for floating offshore wind turbines. Proc. ASME 2016 35th Int. Conf. on Ocean, Offshore and Arctic Eng. (OMAE2016), Busan, South Korea, Vol. 6, Paper No. V006T009A042. http://doi.org/10.1115/OMAE2016-54476

Herduin, M. (2019). Multi-directional loading on shared anchors for offshore renewable energy: definition and preliminary investigation into soil behaviour and anchor performance. PhD thesis, The University of Western Australia, Crawley, WA, Australia.

Herduin, M., Gaudin, C., Cassidy, M.J., O'Loughlin, C.D. and Hambleton, J.P. (2016). Multi-directional load cases on shared anchors for arrays of floating structures. Proc. 3rd Asian Wave and Tidal Energy Conference (AWTEC 2016), Singapore, pp. 1–9

Lovera, A., Coquio, T. and Peyrard, C. (2025). Analysis of loads applied on floating wind turbines shared anchors. Ocean Engineering, 324: 120627. http://doi.org/10.1016/j.oceaneng.2025.120627

Mohr, H., Gaudin, C. and Bransby, M.F. (2022). The use of fiber optic and image analysis to investigate the performance of piles in sand under multi-directional horizontal loading. Proc. 10th International Conference on Physical Modelling in Geotechnics (ICPMG 2022).

Pillai, A.C., Gordelier, T.J., Thies, P.R., Dormenval, C., Wray, B., Parkinson, R. and Johanning, L. (2022). Anchor loads for shallow water mooring of a 15 MW floating wind turbine — Part I: chain catenary moorings for single and shared anchor scenarios. Ocean Engineering, 266: 111816. http://doi.org/10.1016/j.oceaneng.2022.111816

Rashidi Mehrabadi, A., Cerfontaine, B., Gourvenec, S. and White, D.J. (2025). Numerical investigation of multidirectional response of shared anchor piles for offshore wind. Proc. 5th Int. Symp. on Frontiers in Offshore Geotechnics (ISFOG 2025), Nantes, pp. 2447–2453. http://doi.org/10.53243/ISFOG2025-293

Rose, D.T. (2023). Wind-wave misalignment effects on multiline anchor systems for floating offshore wind turbines. MSc thesis, University of Massachusetts Amherst, Amherst, MA, USA.

Soriano-Camelo, C.Y., Thorel, L. and Blanc, M. (2024). Centrifuge modelling of the loading capacity of suction anchors in soft clay: towards multidirectional load. Proc. 5th European Conf. on Physical Modelling in Geotechnics (ECPMG 2024), Delft, The Netherlands, pp. 1–6. http://doi.org/10.53243/ECPMG2024-17

White, D.J., Cerfontaine, B., Rashidi Mehrabadi, A. and Gourvenec, S. (2026). Definitions and characteristics of loading patterns on single and shared marine anchors for floating offshore wind turbines. Applied Ocean Research, Vol. 168: 104980. https://doi.org/10.1016/j.apor.2026.104980

Zabatta, R., Abadie, C.N., Blanc, M., Lerat, S. and Jagu, A. (2025). Centrifuge modelling of intermediate piles subjected to multidirectional cyclic lateral loading. Proc. 5th Int. Symp. on Frontiers in Offshore Geotechnics (ISFOG 2025), Nantes, France, pp. 2348–2354. http://doi.org/10.53243/ISFOG2025-318